Journal of Hazardous Materials 211–212 (2012) 332–341

Contents lists available at SciVerse ScienceDirect

Journal of Hazardous Materials

journal homepage: www.elsevier.com/locate/jhazmat

Immobilization of As(III) in soil and groundwater using a new class of polysaccharide stabilized Fe–Mn oxide nanoparticles

Byungryul An, Dongye Zhao*

Environmental Engineering Program, Department of Civil Engineering, Auburn University, Auburn, AL 36849, USA

ARTICLE INFO

Article history:
Received 2 June 2011
Received in revised form 23 October 2011
Accepted 24 October 2011
Available online 10 November 2011

Keywords:
Arsenic
Arsenite
Metal immobilization
Nanoparticles
Water treatment
Soil remediation

ABSTRACT

A new class of stabilized Fe–Mn binary oxide nanoparticles was prepared with a water-soluble starch or carboxymethyl cellulose (CMC) as a stabilizer. The nanoparticles were characterized and tested with respect to sorption of As(III) and As(V) from water and for immobilization of As(III) in soil. While arsenic sorption capacities were comparable for bare, or stabilized Fe–Mn nanoparticles, particle stabilization enabled the nanoparticles to be delivered into soil for *in situ* immobilization of arsenite. High As(III) sorption capacity was observed over a broad pH range of 5–9. Column breakthrough tests demonstrated soil mobility of CMC-stabilized nanoparticles. Once delivered, the nanoparticles remain virtually immobile in soil under typical groundwater conditions, serving as a fixed sink for arsenic. When an As(III)-laden soil was treated with CMC-stabilized Fe–Mn at an Fe-to-As molar ratio of 6.5–39, the water leachable arsenic was reduced by 91–96%, and the TCLP leachability was reduced by 94–98%. Column elution tests of an As(III)-laden soil indicated that application of CMC-stabilized Fe–Mn transferred nearly all water-soluble As(III) to the nanoparticle phase. Consequently, As(III) is immobilized as the nanoparticles are immobilized in the soil. The nanoparticle amendment was able to reduce the TCLP leachability of As(III) remaining in the soil bed by 78%.

1. Introduction

With growing knowledge on arsenic toxicity, regulations on arsenic (As) in drinking water have been mounting worldwide. In January 2006, the U.S. Environmental Protection Agency (EPA) enforced a revised maximum contaminant level (MCL) of 10 μg/L As in drinking water. This 5-fold tightened MCL has been affecting thousands of water utilities in the U.S. and requires development of more cost-effective treatment technologies.

Among the most cited As removal technologies are adsorption, enhanced coagulation, membrane filtration, and electrolysis [1]. While quite promising, most of the technologies are more effective for removing As(V) than for As(III). For example, standard anion exchanger resins can only remove As(V) oxyanions under typical groundwater conditions [2]. Hering et al. [3], and Jang et al. [4] studied the removal of As(V) and As(III) from water through enhanced precipitation/coprecipitation, and adsorption by hydrous ferric oxide (HFO), respectively. Their results revealed that the removal efficiency of As(III) is generally less than that of As(V), and competitive As(III) and As(V) removal was only observed at alkaline pH when arsenite is dissociated. As a result, additional oxidation units are often required to convert As(III) to As(V).

Scott and Morgan [5] studied As(III) oxidation rate using synthetic birnessite (δ-MnO_2). Despite the low As(III) adsorption capacity of manganese dioxide itself [6], manganese in natural systems is known to play an important role in oxidation of As(III) [7]. The oxidative removal capacity of As(III) was reported to be 7.5 mg/g for synthesized birnessite [7] and 13.5 mg/g for manganese dioxide [8]. By virtue of the oxidation effect of manganese and the high sorption capacity of iron oxides toward arsenate, Zhang et al. [9] reported that the removal of As(III) can be enhanced by applying a binary Fe–Mn oxide adsorbent.

In recent years, iron based nanoscale particles have enticed great interest for water treatment and environmental remediation [10–12]. However, the nanoparticles tend to aggregate rapidly into micro- to millimeter scale aggregates, losing their unique advantages such as high specific surface area and soil deliverability. To overcome agglomeration of the nanoparticles and to control the particle size, organic polymers are often employed as a stabilizer, such as starch [12,13] carboxymethyl cellulose (CMC) [14,15]. The stabilizers attached on the nanoparticles prevent the particles from aggregation through steric and/or electrostatic stabilization mechanisms, leading to improved physical stability, better mobility in soil, and greater specific surface area. Yean et al. [16] observed that the arsenic sorption capacity of magnetite nanoparticles stabilized with oleic acid was 4.6 times greater than a commercial powder magnetite. Furthermore, particle stabilization enables the nanoparticles to be delivered to the contaminated subsurface zones,

* Corresponding author. Tel.: +1 334 844 6277; fax: +1 334 844 6290.
E-mail addresses: zhaodon@auburn.edu, dzhao@eng.auburn.edu (D. Zhao).

0304-3894/$ – see front matter © 2011 Elsevier B.V. All rights reserved.
doi:10.1016/j.jhazmat.2011.10.062

facilitating *in situ* remediation of contaminated soil and groundwater. For example, stabilized zero valent iron (ZVI) nanoparticles have been tested at several contaminated sites and shown to be deliverable into the contaminated source zones [17,18]. Our previous work also revealed that stabilized nanoparticles such as ZVI [15] and FeS [19] may be used for *in situ* immobilization of chromate and mercury in contaminated soils, respectively. The *in situ* remediation technology through injection of nanoparticles not only holds the potential to cut down the remediation cost substantially, but represents an innovative approach to tackle contaminants located in otherwise hardly reachable aquifer zones such as in deep aquifer or aquifers underneath a city or other developed areas.

The overall goal of this research was to investigate the feasibility of using a new class of starch- or CMC-stabilized Fe–Mn oxide nanoparticles (denoted as Fe–Mn) for *in situ* immobilization or removal of both As(III) and As(V) in contaminated soils. The specific objectives of this work were to: 1) prepare and characterize a new class of starch- or CMC-stabilized Fe–Mn nanoparticles, 2) determine the effectiveness of the stabilized nanoparticles for As(III) and As(V) removal from water, 3) examine deliverability of the stabilized Fe–Mn nanoparticles in a model soil, and 4) test effectiveness of the stabilized Fe–Mn nanoparticles for immobilizing As(III) in a contaminated soil.

2. Materials and methods

2.1. Chemicals

Chemicals used in this research were in the analytical grade or higher. $FeSO_4{\cdot}7H_2O$, $KMnO_4$, and sodium carboxymethyl cellulose (CMC, M.W: 90,000) were purchased from Acros Organics (Morris Plains, NJ, USA). A hydrolyzed potato starch and $Na_2HAsO_4{\cdot}7H_2O$ were obtained from Sigma–Aldrich (Milwaukee, WI, USA). $NaAsO_3$ and $MnCl_2$ were purchased from Fisher Scientific (Pittsburgh, PA, USA). All solutions were prepared with ultrapure deionized (DI) water (18.2 $\Omega\,cm^{-1}$).

2.2. Preparation of stabilized Fe–Mn nanoparticles

The stabilized Fe–Mn oxide nanoparticles were prepared by modifying the method by Zhang et al. [30]. The key modification was to apply a low-cost and "green" polysaccharide stabilizer (starch or CMC) during the particle formation. The nanoparticles were fabricated in the following steps. First, prepare a 1 wt.% stock solution of starch and a 1 wt.% CMC stock solution (proper heating was needed to dissolve starch in water). Then, take a desired volume (from 0 to 28 mL) of the starch or CMC solution and dilute with DI water to 120 mL, and mix for 10 min. Prepare an $FeSO_4{\cdot}7H_2O$ solution of 13.9 g/Land another solution of 2.65 g/L of $KMnO_4$ in DI water, and then add 10 mL of the $FeSO_4{\cdot}7H_2O$ solution into 120 mL of a stabilizer solution and mix for 15 min. The redox reaction was then initiated by adding 10 mL of the $KMnO_4$ solution into the mixture of iron sulfate and one of the stabilizers under vigorous magnetic stirring. Immediately increase the pH of the mixture to ~7.5 using 4 M NaOH, and shake the mixture on a platform shaker (New Brunswick Scientific, NJ, USA) at 200 rpm for 1 h. Fe–Mn nanoparticles were then obtained as either precipitates or fully stabilized suspension depending on the concentration and type of the stabilizers present. The Fe–Mn particles were tested or analyzed within 1 h of preparation.

2.3. Physical characterization of Fe–Mn nanoparticles

XRD patterns of bare, and starch-or CMC-stabilized Fe–Mn nanoparticles were obtained using a MiniFlex X-ray diffractomer (Rigaku, Japan) equipped with Cu K-alpha radiation. The nanoparticles were first prepared at 0.27 g/L as total Fe–Mn, and then separated from water and vacuum-dried. The dried samples were ground to a homogenous mixture using a mortar and pestle and then affixed to glass microscope slides upon cleaning the slides using acetone. The samples were diffracted over a 2θ range from 10° to 90°. The Zeta potential (ζ) of the particles was measured with a Zetasizer nano ZS (Malvern Instruments, UK) at 25 °C. Typically, 0.75 mL of a nanoparticle suspension of 0.27 g/L of Fe–Mn was filled in a folded-capillary cell and then measured. For bare Fe–Mn nanoparticles the samples were first sonicated with a sonicator (550 Dismembrator, Fisher Scientific, Pittsburg, PA, USA) right before the measurements. Fourier transform infrared spectroscopy (FTIR) was performed to determine arsenic adsorption mechanisms and interactions between the stabilizers (CMC and starch) and the Fe–Mn oxide nanoparticles. FTIR spectra were obtained for neat CMC and starch samples as well as for bare, CMC- or starch-stabilized Fe–Mn nanoparticles before and after adsorption of arsenate or arsenite. The samples were first vacuum-dried, and then ground in a mortar to fine powders, which were then mixed with KBr at a sample-to-KBr ratio of 5:95 by weight. The mixtures were pressed into thin films with a hydraulic press at 9 metric tons for 2 min. The specimen were then scanned and characterized using an IR Prestige-21 spectrometer (Shimadzu, Japan) over the wave number ranging from 400 to 4000 cm^{-1}.

2.4. Kinetic tests

Batch kinetic tests were conducted to test arsenic sorption rates of the nanoparticles. First, Fe–Mn particles or suspensions were prepared at 0.27 g/L as Fe–Mn (Fe = 0.2 and Mn = 0.07 g/L) in the presence of 0, 0.16 wt.% CMC or 0.19 wt.% starch. Then, the sorption tests were initiated by adding an As(III) stock solution to the nanoparticle suspensions, which resulted in the following conditions: suspension volume = 140 mL, initial As(III) concentration = 100 mg/L, initial pH 5.0. The solution pH was kept at 5.0 ± 0.1 during the tests through intermittent adjustment using 0.1 M NaOH or HCl. The vials were then placed on a platform shaker operated at 200 rpm. At predetermined times, samples were taken at 4 mL each and passed through a 25 nm membrane filter (0.025 μm VSWP, Millipore, USA). The filtration was able to remove all nanoparticles but not any dissolved arsenic. The filtrate was then acidified with one drop of 1 M nitric acid, and then analyzed for arsenic remaining in the aqueous phase.

2.5. As(III)/As(V) adsorption equilibrium tests

A series of batch equilibrium tests were performed to determine the arsenic removal effectiveness with bare and stabilized Fe–Mn nanoparticles. To test the effect of stabilizers on the sorption capacity, Fe–Mn nanoparticles were synthesized at 0.27 g/L as Fe–Mn with various concentrations (0–0.26 wt.%) of starch or CMC and then, arsenic adsorption was initiated by adding a known mass of As(III) or As(V) to yield an initial concentration of arsenic of 100 mg/L. The pH of the suspension was maintained at 5.5 during the tests through intermittent adjusting. The mixtures were equilibrated for 2 days under shaking at 200 rpm. Then, samples were taken, filtered and analyzed for arsenic remaining following the same method as described above.

Batch isotherm tests were performed for As(III) and As(V) adsorption following the similar procedure. The following conditions were applied: initial As = 0–140 mg/L, suspension volume = 140 mL, CMC (sodium form) = 0.16 wt.%, Fe–Mn = 0.27 g/L. The isotherms were constructed at two pH levels of 5.5 and 3.0, which were maintained through intermittent adjustments.

To further investigate the pH effect on arsenic sorption, batch adsorption equilibrium tests were carried out over abroad pH range from 2 to 10 for bare and stabilized (with either 0.16 wt.% CMC or 0.19 wt.% starch) Fe–Mn but under otherwise identical conditions, i.e. initial As = 100 mg/L and Fe–Mn = 0.27 g/L.

2.6. Preparation of As(III)-spiked soil

A sandy soil was obtained near the Auburn University's E.V. Smith Research Center in Tallassee, AL, USA. Prior to use, the sandy soil was washed with tap water several times to remove all soluble components such as dissolved organic matter and other soluble impurities until the supernatant was clear. The sandy soil was air-dried at room temperature and then sieved through a 2-mm screen. The soil was then digested following U.S. EPA method 3050B and analyzed for metals, which gave the following background metal concentrations: Fe = 758 mg/kg, Ca = 240 mg/kg, and Mg = 179 mg/kg. To prepare the As(III) spiked samples, 800 g of the air-dried sandy soil was added into 1 L of As(III) solution containing 150 mg/L as As. The mixture was continuously shaken at pH 6 for 2 weeks to reach equilibrium. Upon equilibrium, the supernatant was decanted and the soil was air-dried and stored for uses. The As(III) loading on the soil was 103.5 mg of As(III)/kg of dry soil.

2.7. As(III) immobilization in soil: batch tests

To investigate the nanoparticles' effectiveness for immobilization of As(III) in the soil, a series of batch tests were carried out by amending the As(III)-spiked soil with stabilized Fe–Mn nanoparticles. In each test, 2 g of the air-dried As(III)-loaded soil was mixed with 30 mL of a suspension of the Fe–Mn nanoparticles stabilized with either 0.16 wt.% CMC or 0.19 wt.% starch in 30 mL Corning plastic centrifuge tubes. The nanoparticle dosage was varied from an Fe-to-As molar ratio of 0–6.5, 13, 26, and 39. The mixtures were rotated using an end-to-end rotator at 30 rpm at room temperature ($21 \pm 0.1\,^{\circ}C$) for 4 days to reach equilibrium at pH 5.5. After 4 days of equilibration, aliquots of the suspensions were sampled and centrifuged at 6500 rpm (5857 *g* of RCF) for 15 min, and then the supernatant was filtered through a 25 nm membrane filter to remove the nanoparticles. Finally, the filtrate was analyzed for As, which gave the total leachable As(III) in the system. To compare the effect of the stabilized Fe–Mn nanoparticles on the leachability of the soil-sorbed As(III), As(III) desorption tests were also carried out in the absence of the nanoparticles by mixing the As(III)-loaded soil with a simulated groundwater (SGW) prepared following the method by Lien and Wilkin [20].

2.8. Fixed-bed column tests

Fixed-bed column tests were conducted to evaluate soil mobility and breakthrough behaviors of the stabilized Fe–Mn nanoparticles and the potential for the attempted *in situ* immobilization of As(III) in contaminated soils. Approximate 9 g of the air-dried sandy soil (without As(III) loaded) was packed in a Plexiglas column (inner diameter = 1.0 cm and length = 10 cm; Omnifit, Cambridge, UK), resulting in a soil bed porosity of 0.40 and a bulk bed volume of 6.4 mL. The CMC-stabilized Fe–Mn nanoparticle suspension was then passed through the soil-packed column at a flow rate of 0.18 mL/min in the down-flow mode, which translated into an empty bed contact time (EBCT) of 35.6 min and a superficial liquid velocity (SLV) of 3.8×10^{-5} m/s. The effluent samples were collected with a fraction collector (EldexLaboraries, Napa, CA, USA), and then completely acidified using 0.1 M HCl and analyzed for total Fe, which was used to represent the concentration of the nanoparticles in the effluent. For comparison, a tracer test was performed using a KBr solution (50 mg/L as Br^-) under identical operating conditions.

To evaluate the effectiveness of the nanoparticles for *in situ* As(III) immobilization, column elution tests were carried out under the same hydrodynamic conditions. To this end, ~9 g of As(III)-loaded soil was packed in the column, then the soil bed was treated by passing 22 pore volumes (PV) of a suspension containing CMC-stabilized Fe–Mn nanoparticles (Fe–Mn = 0.27 g/L, CMC = 0.16 wt.%). The effluent samples were then analyzed in two ways. First, the samples were acidified with 5 M of HNO_3 to completely dissolve the nanoparticles, and then analyzed for total As (adsorbed and free As) in the effluent; Second, the samples were first filtered using a 25 nm membrane filter to remove all the nanoparticles and then the filtrate analyzed for the free or soluble As. For comparison, As(III) elution from the As-loaded soil using the simulated groundwater was also performed in parallel.

2.9. Leachability of As(III) in soil

The toxicity characteristic leaching procedure (TCLP) specified in EPA Method 1311 was employed to determine the leachability of arsenite from untreated and nanoparticle amended soil. Soil samples treated by Fe–Mn nanoparticles or subjected to SGW after the batch or column tests were first air-dried at room temperature and then mixed with the #1 TCLP fluid (pH 4.93) at a solid-to-solution ratio of 1:20 (i.e. 2 g dried soil and 40 mL of #1 TCLP fluid). The mixtures were rotated for 18 h at 30 rpm and then centrifuged at 6500 rpm (5857 *g* of RCF) for 20 min. Arsenic leached in the supernatants was then analyzed. All tests were conducted in duplicate.

2.10. Chemical analyses

Solution or suspension pH was measured using an Oakton pH meter (pH 510 Benchtop Meter, Oakton, CA, USA). Arsenic was analyzed with a Perkin Elmer Graphite Furnace Atomic Absorption Spectrometer, which has a detection limit (DL) of 3 μg/L as As. Concentration of iron and manganese were measured using an ICP-AES (Liberty-SERIES II, Varian, USA)(DL of <5 μg/L for both Fe and Mn). Bromide was analyzed using a Dionex Ion Chromatograph (Model DX-20) equipped with an AS14 column (DL < 0.05 mg/L Br^-).

3. Results and discussion

3.1. Characterization of Fe–Mn nanoparticles by XRD and FTIR

XRD patterns (not shown) for bare, and CMC-or starch-stabilized Fe–Mn nanoparticles revealed no significant peaks (intensity), indicating the non-crystalline nature for these binary Fe–Mn oxides [21]. These results are in accordance with work by Zhang et al. [9] who studied Fe–Mn particles prepared similarly but without starch and CMC, and suggest that the Fe–Mn oxide particles are in the more stable amorphous form. Based on XPS spectra for bare Fe–Mn, Zhang et al. [9] identified that Fe and Mn exist in the oxidation states of (III) and (IV), respectively. Our attempt failed to acquire TEM (transmission electron microscopy) images of the fully stabilized Fe–Mn nanoparticles. Based on DLS (dynamic light scattering) measurements, the hydrodynamic diameter was 348 ± 46 (standard deviation) nm and 247 ± 9 nm for the CMC-and starch-stabilized Fe–Mn nanoparticles, respectively.

Fig. 1 shows the FTIR spectra of neat CMC and starch as well as bare and stabilized Fe–Mn nanoparticles. Fig. 1a compares the characteristics of the stretching frequencies for neat stabilizers and the corresponding stabilized Fe–Mn nanoparticles. Two peaks at 3444 cm^{-1} and 3430 cm^{-1} were found for neat starch and CMC, respectively, and a peak at 3400 cm^{-1} was detected for both types of stabilized Fe–Mn nanoparticles. These peaks correspond to O–H

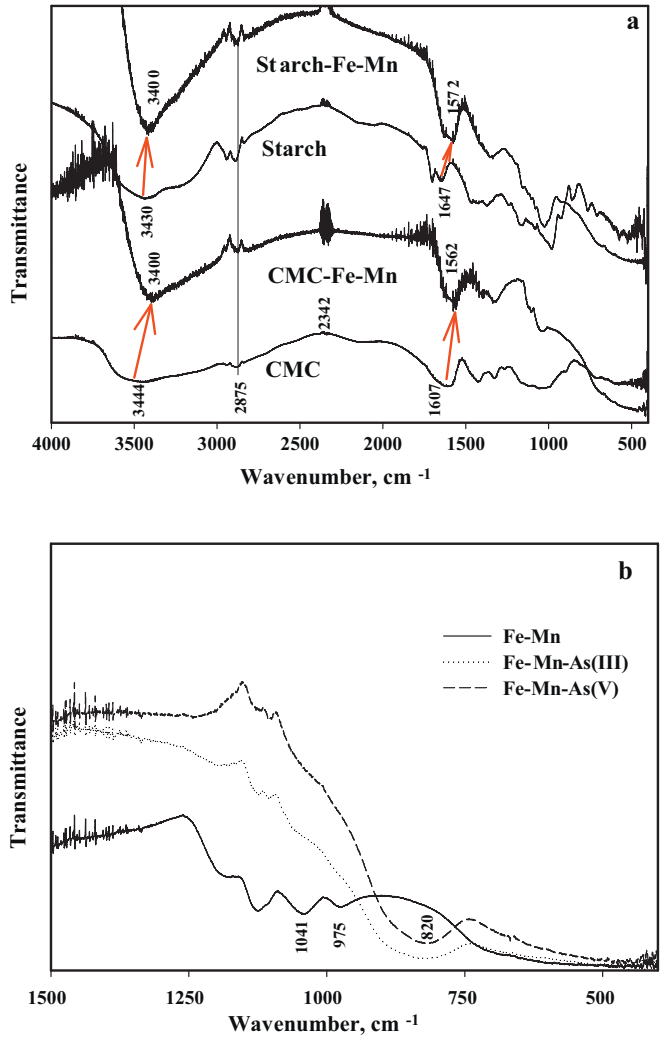

Fig. 1. FTIR spectra of (a) neat CMC and starch, and CMC- or starch-stabilized Fe–Mn nanoparticles (arrows indicate shifts of the peaks), (b) non-stabilized Fe–Mn particles with or without arsenic sorbed.

stretching bond from H_2O, CMC or starch, which agrees with Maity and Agrawal [22] who studied interactions between iron oxide and oleic acid. Upon sorption of the stabilizers to the Fe–Mn particles, a shift was observed from 3444 to 3400 cm^{-1} for CMC-stabilized Fe–Mn and from 3430 to 3400 cm^{-1} for starch-stabilized Fe–Mn. Such a shift can be attributed to the increased strength of intermolecular hydrogen bonds between the stabilizers and surface of the Fe–Mn particles [23,24]. Given the abundance of –OH groups in both CMC and starch, this type of hydrogen bonding can be important in binding the stabilizers to the Fe–Mn particles. The peaks observed at around 2875 cm^{-1} for all four cases indicate the C-H stretching vibrations from the CH_2 groups of the stabilizers [22]. Fig. 1a reveals a shift from 1607 cm^{-1} for neat CMC to 1562 cm^{-1} for CMC-stabilized Fe–Mn. Si et al. [25] reported the same shift and ascribed it to the decrease in the strength of the covalent bond resulting from the inhibition of conjugation of COO^- when attached to a particle surface. Fig. 1a also shows a shift from 1647 cm^{-1} for neat starch, which is due to O–H bond from water, to 1572 cm^{-1} for starch-stabilized Fe–Mn, indicating that more water molecules were bound on the surface of Fe–Mn particles [26,27]. Jones et al. [28] showed that monodentate and bidentate chelating was operative between the carboxylate groups of CMC and surface Fe. However, in the present work, such interaction was not evident based on the FTIR spectra.

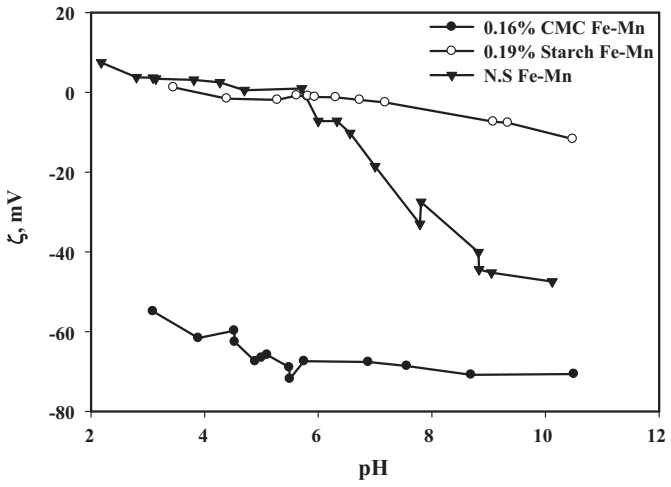

Fig. 2. Zeta potential as a function of pH for bare and stabilized Fe–Mn nanoparticles. Fe–Mn = 0.27 g/L.

Fig. 1b shows FTIR spectra for bare Fe–Mn particles before and after uptake of As(III) or As(V). FTIR studies of various iron oxides have been widely reported, and the following characteristic wave numbers have been reported: 580 cm^{-1} for magnetite [29], 560 cm^{-1} for ferrihydrite film [30], and 441 and 580 cm^{-1} for low crystalline ferrihydrite or amorphous iron(III)-hydroxide [31]. However, the FTIR spectra in Fig. 1 did not show any of these peaks. Instead, two new peaks in Fig. 1b were evident at 1041 and 975 cm^{-1}, respectively. Apparently, the presence of Mn in iron oxide reduced the band strength of Fe–O groups. The two new peaks could be ascribed to Fe–OH based on similar observations reported by Zhang et al. [29] who studied Fe–Ce binary metal oxides for arsenate adsorption. They observed that the intensity of Fe–O peak at 580 cm^{-1} was progressively weakened as the Ce concentration was raised, and the peak became undetectable at an Fe:Ce molar ratio of 3:1, where two new peaks at 1126 and 1067 cm^{-1} appeared representing the Fe–OH groups [32]. Fig. 1b shows that the Fe–OH peaks disappeared upon uptake of As(III) or As(V) to the bare Fe–Mn particles. Furthermore, the sorption of arsenic gave rise to a new broad band at 820 cm^{-1} corresponding to As–O stretching vibration, which is characteristic of As(V) sorption [29,30,33]. For As(III) sorption to bare Fe–Mn, Zhang et al. [34] observed a peak at 577 cm^{-1}, which was attributed to the As–O vibration. However, in this work, the peak was not detected for bare or stabilized Fe–Mn particles. Based on this observation and the presence of the strong broad peaks at 820 cm^{-1} for both As(III)- and As(V)-laden Fe–Mn, it is evident that As(III) was, at least in part, first oxidized to As(V) and then adsorbed onto the surface of the Fe–Mn oxides. Pena et al. [35] compared FTIR bands for sorbed and dissolved arsenate species and observed that two peaks at 878 and 909 cm^{-1} for dissolved $H_2AsO_4^-$ corresponding to the symmetric and asymmetric stretching vibrations of As–O bonds, respectively. Upon adsorption, the peaks were shifted to 808 and 830 cm^{-1}, respectively. According to Goldberg and Johnston [33] and Pena et al. [35], the shift on band positions was attributed to symmetry reduction resulting from inner-sphere complex formation (i.e. formation Fe–O–As complexes). In our study, the presence of the one broad band at 820 cm^{-1} suggests that similar surface complexation is the predominant mechanism for arsenate sorption to the Fe–Mn particles.

3.2. *Effect of stabilizers on zeta potential of Fe–Mn nanoparticles*

Fig. 2 shows the measured zeta potential (ζ) as a function of pH for bare and stabilized Fe–Mn particles. Evidently, coating of the neutral starch and negatively charged CMC molecules ($pK_a = 4.3$)

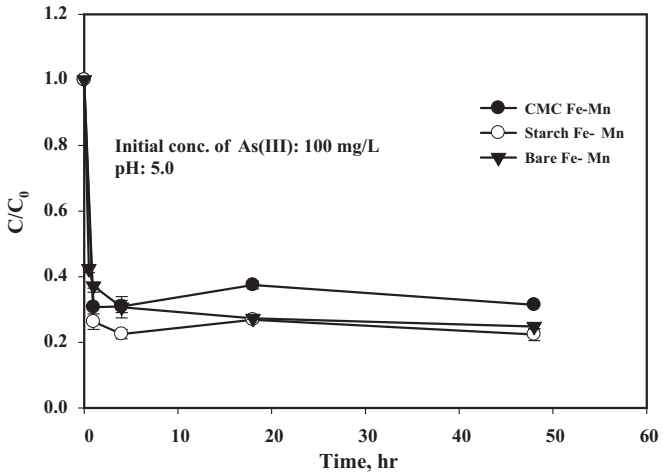

Fig. 3. Arsenite removal as a function of time using bare or stabilized Fe–Mn nanoparticles under otherwise identical conditions. Experimental conditions: CMC = 0.16 wt.% for CMC-stabilized particles; Fe = 0.20 g/L; Mn = 0.07 g/L; starch = 0.19 wt.% for starch-stabilized particles. Solution pH was kept at 5.0 in all cases. Data are plotted as mean of duplicate, errors indicate standard deviation from the mean.

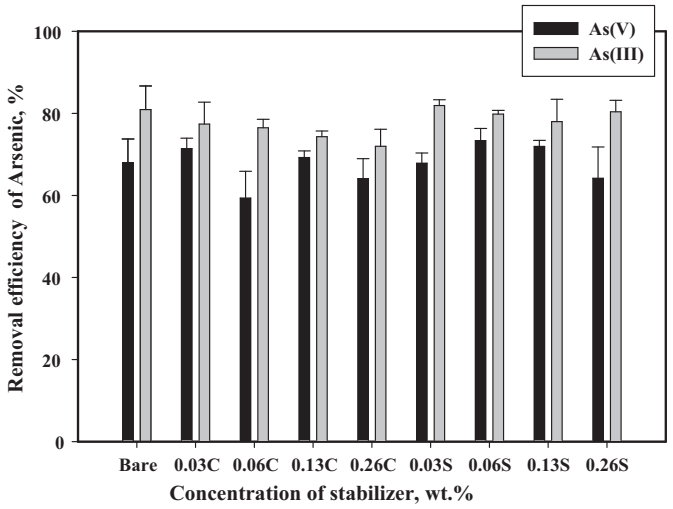

Fig. 4. Arsenic removal as a function of type and concentrations of a stabilizer. Experimental conditions: Fe = 0.2 g/L; Mn = 0.7 g/L; pH 5.5; initial As(V) = 100 mg/L; and initial As(III) = 108 mg/L of As(III). (Notations: Bare: non-stabilized Fe–Mn particles, C: CMC, S: starch; numbers refer to wt.% of a stabilizer added.)

greatly altered the ζ value over a broad pH range. For the bare Fe–Mn binary oxides, the ζ value underwent a sharp change from +2 to −45 mV over the pH range of 5.7–8.9, which revealed a point of zero charge (PZC) pH of ~6. Kosmulski et al. [36] reported PZC values of 8.32 and 7.99, respectively, for goethite and Fe(III) hydroxides. Su and Suarez [37] reported a PZC of 8.5 for synthetic amorphous $Fe(OH)_3$. For synthetic birnessite (δ-MnO_2), the PZC was reported to fall in a typical range from 1.5 to 2.5 [38,39]. Comparing the ζ–pH profile of bare Fe–Mn and those of typical iron oxide minerals, it appears that $Fe(OH)_3$ dominates the characteristics of the Fe–Mn binary oxides. In the presence of 0.19 wt.% of starch, however, the surface potential was largely shielded. Over the pH range of 3.3–7.2, ζ was nearly zero, and it was only changed to −10 mV when pH was extended to 10.5. Evidently, the presence of starch, which is a neutral polymer with dense H-bonding [40,41] results in a strong surface "buffer" that diminishes the effect of H^+/OH^- on the surface charge. This is plausible given that the starch macromolecules have pre-occupied the functional sites of the core Fe–Mn particles, which impedes protonation or deprotonation of these functional groups. In contrast, in the presence of 0.16 wt.% of CMC, ζ was substantially lowered to below −50 mV throughout the pH range (<−65 mV at pH >5). From the particle stabilization viewpoint, the surface potential values indicate that steric stabilization is the predominant mechanism for starch, while electrosteric stabilization is operative for CMC, i.e. CMC is likely to be a more effective stabilizer than starch. With respect to arsenic sorption, however, the highly negative surface charge induced by CMC would tend to exclude the arsenate anions, which is expected to offset, at least in part, the benefit of greater specific surface area of the nanoparticles.

3.3. As(III) sorption kinetics

Fig. 3 shows As(III) sorption rates of bare and CMC- or starch-stabilized Fe–Mn particles at a fixed nanoparticle dosage of 0.27 g/L as Fe–Mn. For stabilized Fe–Mn particles, equilibrium was reached within 1 h, whereas for bare Fe–Mn particles, the sorption was characterized with a rapid initial (<4 h) followed by a rather slow uptake phase. The equilibrium As(III) removal was 69%, 75%, and 77% for CMC-stabilized, bare, and starch-stabilized Fe–Mn, respectively. In terms of sorption capacity, the results appear to be counter-intuitive. While stabilized particles are expected to offer much greater surface area, the particle stabilization did not offer the expected capacity hike. In fact, the capacity for CMC-stabilized particles was 6% lower than for the bare particles. Apparently, while these stabilized nanoparticles offer comparably greater specific area, the stabilizers on the particle surface may inhibit arsenic uptake both thermodynamically (due to reduced sorption sites and site accessibility) and kinetically (due to increased mass transfer resistance). In addition, coating the nanoparticles with the stabilizers also greatly alters the surface potential, which can also affects sorption of the arsenic species. For CMC-coated Fe–Mn nanoparticles, the highly negative surface potential (Fig. 2) renders sorption of As(V) oxyanions (resulting from partial oxidation of As(III)) a unfavorable process. From a soil remediation standpoint, however, the particle stabilization is of great significance. As to be shown later, the stabilizers prevent the nanoparticles from aggregation and enable the particles to be deliverable into contaminated soil.

3.4. Effect of stabilizers on equilibrium uptake and particle stability

Fig. 4 shows the percentage removal of As(III) and As(V) as a function of type and concentration of stabilizers. The average removal of As(III) was 81, 80, and 75% for bare, starch-, and CMC-stabilized Fe–Mn particles, respectively. Increasing CMC from 0 to 0.26% progressively reduced the As(III) removal by ~9%. For As(V), the removal rate remained about the same at ~68% for bare and stabilized particles. Again, the presence of the stabilizers did not appear to offer any advantage in terms of sorption capacity for As(III) and As(V). It is noteworthy that the nanoparticles displayed ~10% greater removal for As(III) than for As(V) under the experimental conditions. The same phenomenon was also reported by Zhang et al. [9] and Deschamps et al. [42], who studied arsenic sorption with non-stabilized Fe–Mn particles. Manning et al. [7] ascribed the phenomenon to the creation of more fresh sites upon reduction of MnO_2 by As(III).

Based on particle stability analysis, complete stabilization of 0.27 g/L Fe–Mn nanoparticles was achieved with either 0.19 wt.% starch or 0.16 wt.% CMC. While the arsenic uptake capacities are comparable for bare and fully stabilized nanoparticles, the particle stabilization resulted in discrete, fully dispersible nanoparticles, thereby enabling the nanoparticles to be delivered into contaminated soil to facilitate *in situ* immobilization of arsenic (as to be shown later on). Fig. 5 shows sorption isotherms for As(III) and

Table 1
Model-fitted Langmuir parameters (Q, b).

pH	Arsenic	Q (mg/g) (Standard error)	b (L/mg) (Standard error)
3.0	As(III)	182 (19.9)	0.14 (0.067)
3.0	As(V)	372 (13.0)	0.80 (0.18)
5.5	As(III)	338 (9.5)	0.66 (0.096)
5.5	As(V)	272 (5.1)	0.65 (0.062)

As(V) at pH levels of 5.5 and 3.0 for 0.16 wt.% CMC-stabilized Fe–Mn. The classical Langmuir isotherm model, Eq. (1), was employed to interpret the experimental data. The best data fitting gave the maximum adsorption capacity (Q) and the Langmuir affinity constant (b).

$$q_e = \frac{bQC_e}{1 + bC_e} \quad (1)$$

where q_e is the equilibrium As uptake (mg/g), C_e is the equilibrium concentration of As in water (mg/L), and b and Q are the Langmuir affinity and capacity coefficients, respectively. Table 1 lists the model-fitted b and Q values. The results revealed that sorption of the two arsenic species by Fe–Mn is highly pH dependent, i.e. the sorption capacity for As(III) and As(V) varies with pH. At pH 5.5, the sorbent prefers As(V) over As (III), as has been commonly noted. Despite the inhibitive effect of CMC on the sorption capacity, the fitted b and Q values for the CMC-stabilized Fe–Mn are much greater than those reported for other adsorbents, for examples, 135 mg-As(III)/g for magnetite [16] and 55 mg-As(III)/g for Ce–Ti powder [43]. Moreover, the maximum adsorption capacity is higher than other Fe–Mn products reported in the literature, for example, 138 mg-As(III)/g [44] and 113 mg-As(V)/g [9]. However, at pH 3.0, As(V) becomes much more preferred species over As(III). The Q value for As(V) surpassed that for As(III) by a factor of 2.4.

3.5. Effect of pH

The effect of pH on sorption of As(III) and As(V) onto the Fe–Mn particles was investigated further. Solution pH can affect both the ζ potential of the particles and arsenic speciation. Fig. 6 provides the arsenic sorption profiles over a broad solution pH range. As stated earlier, the dominant mechanism for As(V) adsorption is believed to be surface complexation between Fe and the ligands ($H_2AsO_4^-$ and/or $HAsO_4^{2-}$), forming the Fe–O–As groups. Fig. 6 shows that As(V) sorption increased clearly with decreasing pH.

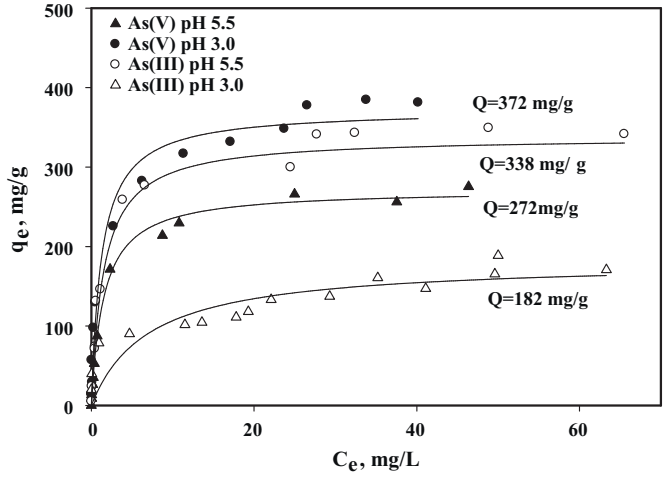

Fig. 5. As(III) and As(V) sorption isotherms for CMC-stabilized Fe–Mn nanoparticles at pH 3.0 and 5.5. (Symbols: observed data; lines: Langmuir model fits.) Initial arsenic = 5–140 mg/L, Fe–Mn = 0.27 g/L as Fe–Mn, CMC in Na form = 0.16 wt.%.

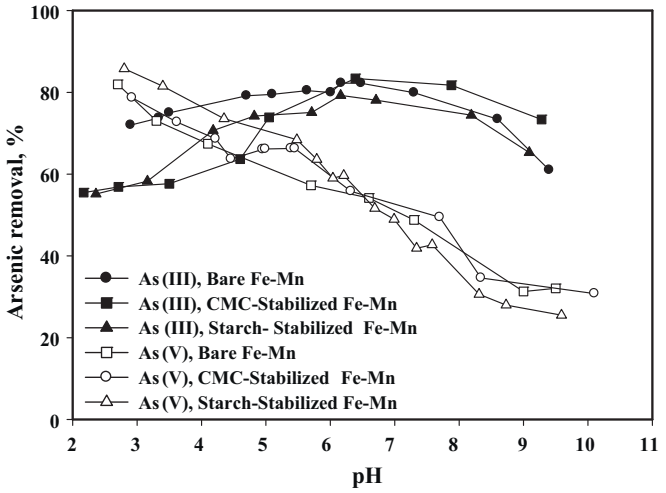

Fig. 6. Equilibrium As(III) and As(V) uptake as a function of solution pH for bare, 0.16 wt.% CMC-, or 0.19 wt.% starch-stabilized Fe–Mn nanoparticles. Initial arsenic = 100 mg/L; Fe = 0.2 g/L; Mn = 0.7 g/L.

At lower pH, more of the surface hydroxyl groups are protonated to OH_2^+, resulting in more and stronger sorption sites for arsenate. At elevated pH, deprotonation of surface hydroxyl groups would result in a negatively charged surface. This unfavorable adsorption condition for As(V) is exacerbated at very alkaline pH (e.g. pH > 9) due to direct competition of OH^- with arsenate [45]. In As(III) sorption, the pH effect displayed a rather different pattern. Solution pH hardly affected As(III) uptake by bare Fe–Mn particles. This is accordance with the fact that in the pH range tested, As(III) existed predominantly as $H_3AsO_3^-$. However, the removal efficiency for both stabilized Fe–Mn nanoparticles at pH <6 was lower than for bare Fe–Mn particles, e.g. 15% lower at pH 3. The capacity drop can be attributed to the dual mechanisms for As(III) removal by MnO_2, i.e. direct uptake of As(III) and oxidation of As(III) to As(V) followed by sorption of As(V). At pH 3.4 and 3.8 in Fig. 6, the concentration of Mn^{2+} in solution was found to be, respectively, 34.4 and 32.2 mg/L for bare Fe–Mn and 27.8 and 24.5 mg/L for CMC-stabilized Fe–Mn. As Mn^{2+} production is coupled with As(III) oxidation, more As(III) was oxidized and then removed as As(V) by bare Fe–Mn than the stabilized counterparts.

In general, As(V) adsorption on amorphous iron oxides decreases with increasing solution pH, and As(III) adsorption on amorphous oxides displays a maximum uptake at around pH 7 [33]. The profiles of As(III) and As(V) sorption by Fe–Mn nanoparticles as a function of pH closely follow these reported patterns, suggesting that iron oxides play a pivotal role in the overall uptake of both As(III) and As(V). However, based on both FTIR (Fig. 1) analysis and discussion (Section 3.6) below, in the presence of MnO_2, As(III) is removed in part in its oxidized form.

3.6. Oxidation of As(III) to As(V) by manganese dioxide

The oxidative sorption process for As(III) removal can be described by the following stoichiometry [34]:

$$MnO_2(s) + H_3AsO_3 + 2H^+ = Mn^{2+} + H_3AsO_4 + H_2O$$
$$E^\circ(V) = +0.67 \quad (2)$$

According to Eq (2), 1 M of $MnO_2(s)$ can oxidize 1 M of As(III), and subsequently, releases 1 M of Mn^{2+} into the aqueous phase. Therefore, the concentration of Mn^{2+} in the solution following As(III) sorption can serve as a measure of the extent to which As(III) is oxidized to As(V). Thermodynamically, this overall reaction is favorable under the experimental conditions. Table 2 shows the

Table 2
Concentration of Fe and Mn in solution after As(III) or As(V) sorption onto various types of Fe–Mn nanoparticles. Experimental conditions (Fe–Mn = 0.27 g/L; initial As(III) = 100 mg/L, initial As(V) = 100 mg/L, pH 5.5).

	As(III)			As(V)		
	Fe (mg/L)	Mn (mg/L)	Released Mn, wt.%	Fe (mg/L)	Mn (mg/L)	Released Mn, wt.%
Non-stabilized Fe–Mn	0.011	9.0	15	0.056	0.046	0.075
Fe–Mn with 0.048 wt.% CMC	0.38	12	20	0.16	0.19	0.31
Fe–Mn with 0.048 wt.% Starch	0.036	9.3	15	0.11	0.11	0.18
Fe–Mn with wt.% CMC	0.47	11	18	0.37	0.72	1.2
Fe–Mn with wt.% Starch	0.018	13	21	0.025	0.14	0.23

concentration of soluble iron and manganese following the sorption of As(III) and As(V). The concentration of dissolved iron was always below 0.47 mg/L in all cases. However, the concentration of manganese ranged from 9 to 13 mg/L for the case of As(III) adsorption, compared to only 0.046–0.72 mg/L for the case of As(V) adsorption. The measured soluble manganese accounted for 14.5–21.0 wt.% of the total Mn in the particles. The presence of either stabilizer showed no effect on the As(III) oxidation at pH 5.5. Manning et al. [7] and Scott and Morgan [5] reported that about 70, 90, 95, and ~100% As(III) was oxidized to As(V) by synthesized birnessite (δ-MnO_2) at a Mn:As molar ratio of 6.2, 44.5, 15, and 29, respectively, within 10 h.

While the presence of soluble Mn^{2+} and As(V) clearly supports the notion that As(III) is at least partially oxidized by MnO_2, quantifying the extent of As(III) oxidation should consider adsorption of Mn^{2+} to the sorbent. Scott and Morgan [5] reported that upon oxidation of As(III) by birnessite, the molar ratio of Mn^{2+}:As(V) was approximately 0.93, suggesting that ~7% Mn^{2+} was sorbed. Based on our Mn^{2+} batch adsorption tests with the Fe–Mn particles (Fe = 0.2 g/L, Mn = 0.07 g/L, initial Mn^{2+} = 90 mg/L), the removal of Mn^{2+} was 7, 15, 27, 83, and 99%, respectively, at a final pH 4.5, 5.6, 5.9, 6.5, and 7.5. Based on these removal rates and the measured aqueous phase Mn^{2+} concentrations, the amount of As(III) oxidized was estimated to be ~25 mg/L (i.e. 25%) under the experimental conditions (pH 5.5, initial As(III) = 100 mg/L, and Fe–Mn = 0.27 g/L).

3.7. Mobility of stabilized Fe–Mn nanoparticles in a sandy soil

For *in situ* immobilization uses, the Fe–Mn nanoparticles must be mobile enough to allow for effective delivery into arsenic contaminated soils. To this end, effective particle stabilization is of paramount importance [14,18]. To preliminarily demonstrate the mobility of the stabilized nanoparticles, column breakthrough tests of the CMC-stabilized Fe–Mn nanoparticles were carried out using a sand soil. Fig. 7 shows the breakthrough curves and elution profiles of the nanoparticles. For comparison, the breakthrough curve for a tracer, Br^-, is also superimposed. The breakthrough of CMC-stabilized Fe–Mn nanoparticles started almost simultaneously with the tracer at ~1 PV (pore volumes) and reached a plateau (complete breakthrough) at ~4 PVs. At full breakthrough, the effluent concentration of iron amounted to ~90% of the influent level, indicating that ~10% of the nanoparticles was consistently retained in the soil bed. Similar breakthrough profiles were observed by He et al. [46] who tested transport of CMC-stabilized ZVI nanoparticles through various porous media [46]. Fig. 7 shows that the nanoparticles are quite mobile under the specified hydrokinetic conditions, and thus, are likely to be deliverable in soil. The observed 10% particle removal can be attributed to the filtration effect. According to the classical filtration theory, particles are transported to the media matrix surfaces by Brownian diffusing, interception, and/or gravitational sedimentation, resulting in partial deposition of particles to the matrix surface [47]. From a practical view point, such soil-associated nanoparticles can serve as a permanent sink for immobilization of arsenic.

Two sets of factors may govern the particle deposition: physical parameters, such as particle size and density, pore fluid velocity, pore structure, and the accessible surface area of the matrix; and the solution and surface chemistry. The hydrodynamic conditions especially pore water velocity can greatly affect particle deposition [46], and thus, manipulating the pore velocity may facilitate particle delivery and control the soil retention of the nanoparticles. The elution curve in Fig. 7 shows that ~36% of the retained nanoparticles was eluted at the same pore velocity, indicating that most of the retained nanoparticles were irreversibly deposited even at the fairly high elution flow rate. Based on our earlier work [46], the nanoparticles, whether retained or not, will most likely remain immobile under typical natural groundwater conditions (i.e. at a much lower pore velocity). Therefore, we expect that once delivered in the subsurface, the CMC-stabilized Fe–Mn nanoparticles will remain nearly immobile and serve as a reactive sink for immobilization of arsenic in soil and groundwater. Starch-stabilized Fe–Mn nanoparticles (Fe–Mn = 0.27 g/L; starch = 0.16 wt.%) were less mobile (data not shown). Nearly all particles were removed at ~10 PVs due to soil clogging. Non-stabilized Fe–Mn particles were not mobile and were all removed on the top of the soil bed.

3.8. Immobilization of As(III): batch tests

The effectiveness of stabilized Fe–Mn nanoparticles for As(III) immobilization in a sandy soil was investigated in batch tests at various dosages of stabilized Fe–Mn nanoparticles. Fig. 8a compares the concentrations of arsenic leached into the solution phase from the As-laden soil in the absence and the presence of various dosages of the nanoparticles. In the absence of nanoparticles (i.e. when the As-laden soil was mixed with the simulated ground water), the released As concentration reached 3800 μg/L. In contrast, when the

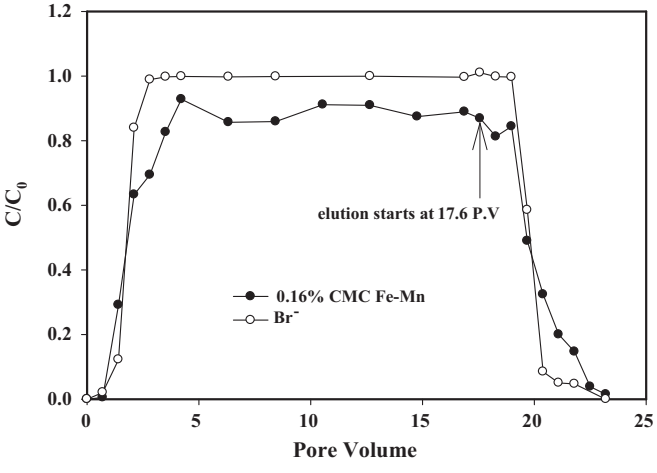

Fig. 7. Breakthrough curves and subsequent elution histories of a tracer (Br^-) and CMC stabilized Fe–Mn nanoparticles through a sandy soil. Experimental conditions: EBCT: 35.6 min, SLV: 3.8×10^{-5} m/s, influent pH 7 ± 0.1, Fe–Mn = 0.27 g/L, CMC = 0.16 wt.%. (Arrow indicates the point where elution was started.)

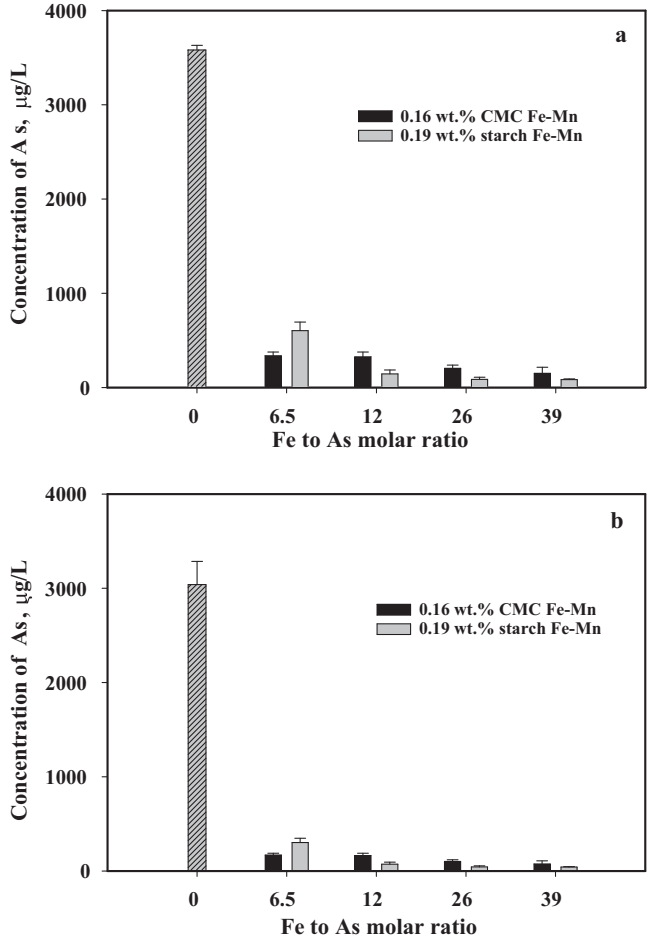

Fig. 8. (a) Arsenic concentration in the aqueous phase when an As(III)-laden soil was amended with water or various doses of stabilized Fe–Mn nanoparticles for 4 days; (b) Arsenic concentration in the TCLP fluid when the soil samples in (a) were subjected to TCLP tests.

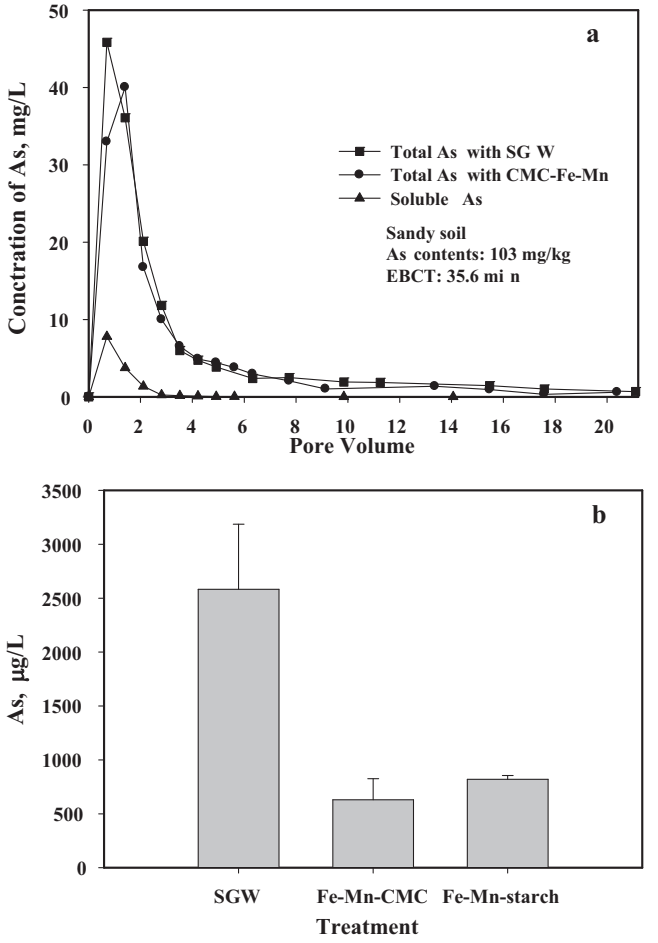

Fig. 9. (a) Arsenic elution profiles using simulated groundwater or CMC-stabilized Fe–Mn nanoparticle suspensions (soluble As refers to As concentration after nanoparticels are removed), and (b) arsenic concentration in the TCLP fluid when the soil samples from (a) were subjected to TCLP tests.

soil was mixed with the nanoparticle suspensions, the leachable As concentration was greatly reduced. For examples, at an Fe:As molar ratio of 6.5, the leached arsenic was reduced by 91% to 336 μg/L with CMC-stabilized Fe–Mn and by 84% to 603 μg/L with starch-stabilized Fe–Mn. When the dosage was increased to Fe:As = 39, the leached As was further reduced by 5% for CMC-stabilized Fe–Mn and 14% for starched nanoparticles. The results clearly demonstrate that both types of the nanoparticles were highly effective to transfer soluble As(III) into the nanoparticle phase. Thus, As(III) can be effectively immobilized as the nanoparticles are deposited in the soil matrix.

To further investigate the leachability of arsenite remaining in the untreated or nanoparticle-amended soil, TCLP leaching tests were performed on the As(III)-laden soil following the batch treatments represented in Fig. 8a. Fig. 8b shows that the TCLP leachable As concentration amounted to 3000 μg/L for the water amended soil. In contrast, the TCLP leachability was reduced by 94–98% for samples treated with CMC-stabilized Fe–Mn at Fe–As of 6.5–39, and by 90–99% with starch-stabilized Fe–Mn. The findings are consistent with the FTIR results. The formation of strong surface complexes between arsenic and the added iron greatly enhanced binding of the arsenic species to the solid phase. In all cases, the nanoparticle amendment rendered the As concentration in the TCLP fluid far below the current threshold concentration of 5 mg/L, which was based on the prior MCL of 0.05 mg/L as As. As a rule, the TCLP threshold is coupled with the corresponding MCL by a factor of 100, and it is believed that the TCLP threshold value is likely to be tightened significantly in the future. To this end, the nanoparticle amendment is of great practical significance for handling of As-laden soil or solid wastes, as it may offer a powerful tool to convert a potentially hazardous waste into a less or non-hazardous material.

3.9. Immobilization of As(III) in soil: column tests

CMC-stabilized Fe–Mn nanoparticles were tested for treating the arsenite-laden sandy soil through fixed-bed column experiments. Fig. 9a compares the arsenic elution histories during two column runs: one with SGW and the other with CMC-stabilized Fe–Mn nanoparticle suspension under otherwise identical conditions. In both cases, the elution curves displayed an immediate peaking followed by a gradual tailing. Based on mass balance, SGW eluted ~17% of arsenic loaded in the soil while Fe–Mn suspension leached ~15%. However, when the effluent samples of the nanoparticle suspension were further examined, ~94% of the eluted As by Fe–Mn suspension was associated with the nanoparticles, while all As eluted by SGW was soluble. Evidently, the nanoparticles converted nearly all water-soluble As into nanoparticle-associated As. Because the nanoparticles are virtually immobile under natural groundwater conditions, i.e. the nanoparticles eluted will be eventually deposited in the soil matrix down the stream once the injection pressure is removed. This is of great practical significance

in reducing As mobility and bioavailability. He et al. [46] showed that under natural groundwater conditions, CMC-stabilized ZVI nanoparticles, which have an iron oxide shell, are mobile under high pore velocities, but immobile when the pressure is removed. Based on the nanoparticle breakthrough curves shown in Fig. 7 and following the modeling approach by He et al. [46], the maximum travel distance of the CMC-stabilized Fe–Mn nanoparticles was estimated to be 2.8 m under a pore groundwater velocity of 0.18 m/s. Consequently, the delivered nanoparticles will serve as an immobile sink for immobilization of water-leachable arsenite.

Following the elution tests, the TCLP leachability for As remaining in the soil samples, which were subjected to SGW or nanoparticle suspension, was determined. Noting that the As mass remaining in the soil bed was about the same after the two elution tests, Fig. 9b shows that the nanoparticle amendment reduced the TCLP leachability by more than 76%, which can be attributed to the added sorption capacity and affinity due to the Fe–Mn nanoparticles retained in the soil. The presence of iron in soil has been known to retain more arsenic in the soil phase. For examples, Hartley et al. [48] reported that iron oxides could facilitate arsenic immobilization at a former landfill site. The results from Fig. 9a and b indicate that the nanoparticle amendment can not only immobilize the groundwater soluble As(III), but reduce the leachability of the remaining As(III) in the soil phase.

4. Conclusions

The main findings and conclusions can be summarized as follows:

- Based on XRD patterns, the starch- and CMC-stabilized Fe–Mn particles were characterized with amorphous structure.
- FTIR analyses showed that As(V) was sorbed to the Fe–Mn particles through inner-sphere surface complexation via Fe–O–As bonding, whereas As(III) was removed via two mechanisms: 1) direct sorption of As(III), and 2) oxidation of As(III) followed by sorption as As(V).
- The stabilized nanoparticles offered comparable arsenic adsorption capacity to bare Fe–Mn particles. Yet, the use of stabilizers enabled the particles to be fully dispersible in water and transportable in soil. The sorbents preferred arsenite over arsenate at pH > 5, but the opposite is true at pH < 4. The maximum Langmuir capacity was determined to be 338 and 272 mg/g for As(III) and As(V) at pH 5.5, respectively, compared to 372 mg/g and 182 mg/g at pH 3.0.
- Sorption of As(III) was less sensitive to pH than that of As(V). High As(III) sorption capacity was observed over broad pH range of 5–9.
- Column breakthrough tests and elution profiles demonstrated the mobility of the CMC-stabilized nanoparticles, and 10% of the nanoparticles were consistently retained in the soil bed. Once delivered, the nanoparticles remain virtually immobile in soil under typical groundwater conditions, serving as a fixed sink for immobilization of arsenic.
- CMC-stabilized Fe–Mn nanoparticles were highly effective for immobilizing arsenic in a sandy soil. When an As(III)-laden soil was treated with CMC-stabilized Fe–Mn at an Fe-to-As molar ratio of 6.5–39, the water leachable arsenic was reduced by 91–96%, and the TCLP leachability of arsenic was reduced by 94–98%.
- Column elution tests of an As(III)-laden soil indicated that application of CMC-stabilized Fe–Mn suspension transferred nearly all water-soluble As(III) to the nanoparticle phase. Consequently, As(III) is immobilized as the nanoparticles are immobilized in the soil matrix. In addition, the simple nanoparticle amendment was able to reduce the TCLP leachability of As(III) remaining in the soil by 78%.

Acknowledgments

This research was partially supported by the Alabama Agricultural Experiment Station Hatch and Multistate Funding program, an EPA STAR Grant (GR832373) and a grant from Vulcan Materials, Inc. We thank Mr. Little for assisting with the powder XRD analyses.

References

[1] H.W. Chen, M.M. Frey, D. Clifford, L.S. McNeil, M. Edwards, Arsenic treatment considerations, J. Am. Water Works Assoc. 91 (1999) 74–85.
[2] D. Clifford, C.C. Lin, Arsenic III and Arsenic V removal from drinking water in San Ysidro, New Mexico, EPA/600/2-91/011. U.S. EPA, Cincinnati, OH, 1991.
[3] J.G. Hering, P-Y. Chen, J.A. Wilkie, M. Elimelech, S. Liang, Arsenic removal by ferric chloride, J. Am. Water Works Assoc. 88 (1996) 155–167.
[4] M. Jang, J.S. Hwang, S.I. Choi, J.K. Park, Remediation of arsenic-contaminated soils and washing effluents, Chemosphere 60 (2005) 344–354.
[5] M.J. Scott, J.J. Morgan, Reactions at oxide surfaces. 1. Oxidation of As(III) by synthetic birnessite, Environ. Sci. Technol. 29 (1995) 1898–1905.
[6] M. Edwards, Chemistry of arsenic removal during coagulation and Fe-Mn oxidation, J. Am. Water Works Assoc. 86 (1994) 64–78.
[7] B.A. Manning, S.E. Fendorf, B. Bostick, D.L. Suarez, Arsenic(III) oxidation and arsenic(V) adsorption reactions on synthetic birnessite, Environ. Sci. Technol. 36 (2002) 976–981.
[8] M. Bissen, F.H. Frimmel, Arsenic – a review. Part II: oxidation of arsenic and its removal in water treatment, Acta Hydrochim. Hydrobiol. 31 (2003) 97–107.
[9] G. Zhang, J. Qu, H. Liu, R. Liu, R. Wu, Preparation and evaluation of a novel Fe-Mn binary oxide adsorbent for effective arsenite removal, Water Res. 41 (2007) 1921–1928.
[10] D.L. Huber, Synthesis properties, and applications of iron nanoparticles, Small 1 (2005) 482–501.
[11] S.R. Kanel, J.M. Greneche, H. Choi, Arsenic(V) removal from groundwater using nano scale zero-valent iron as a colloidal reactive barrier material, Environ. Sci. Technol. 40 (2006) 2045–2050.
[12] B. An, Q. Liang, D. Zhao, Removal of arsenic(V) from spent ion exchange brine using a new class of starch-bridged magnetite nanoparticles, Water Res. 45 (2011) 1961–1972.
[13] F. He, D. Zhao, Preparation and characterization of a new class of starch-stabilized bimetallic nanoparticles for degradation of chlorinated hydrocarbons in water, Environ. Sci. Technol. 39 (2005) 3314–3320.
[14] Y. Xu, D. Zhao, Reductive immobilization of chromate in water and soil using stabilized iron nanoparticles, Water Res. 41 (2007) 2101–2108.
[15] F. He, D. Zhao, Manipulating the size and dispersibility of zerovalent iron nanoparticles by use of carboxymethyl cellulose stabilizers, Environ. Sci. Technol. 41 (2007) 6216–6221.
[16] S. Yean, L. Cong, C.T. Yavuz, J.T. Mayo, W.W. Yu, A.T. Kan, V.L. Colvin, M.B. Tomson, Effect of magnetite particles on adsorption and desorption of arsenite and arsenate, J. Mater. Res. 20 (2005) 3255–3264.
[17] P. Bennett, F. He, D. Zhao, B. Aiken, L. Feldman, In situ testing of metallic iron nanoparticle mobility and reactivity in a shallow granular aquifer, J. Contam. Hydrol. 116 (2010) 35–46.
[18] F. He, D. Zhao, C. Paul, Field assessment of carboxymethyl cellulose stabilized iron nanoparticles for in situ destruction of chlorinated solvents in source zones, Water Res. 44 (2010) 2360–2370.
[19] Z. Xiong, F. He, D. Zhao, M.O. Barnett, Immobilization of mercury in sediment using stabilized iron sulfide nanoparticles, Water Res. 43 (2009) 5171–5179.
[20] H-L. Lien, R.T. Wilkin, High-level arsenite removal from groundwater by zero-valent iron, Chemosphere 59 (2005) 377–386.
[21] X. Chen, C. Quan, W. Wang, Z. Chen, Z. Wu, Z. Wu, X-ray diffraction and X-ray absorption spectroscopy studies on the chemical transformation and formation of nanoscale $LaMnO_{3.12}$, J. Phys. Chem. 111 (2007) 4512–4518.
[22] D. Maity, D.C. Agrawal, Synthesis of iron oxide nanoparticles under oxidizing environment and their stabilization in aqueous and non-aqueous media, J. Magn. Magn. Mater. 308 (2007) 46–55.
[23] J.P. Sylvestre, A.V. Kabashin, E. Sacher, M. Meunier, J.H.T. Luong, Stabilization and size control of gold nanoparticles during laser ablation inaqueous cyclodextrins, J. Am. Chem. Soc. 126 (2004) 7176–7177.
[24] F. He, D. Zhao, J. Liu, C.B. Roberts, Stabilization of Fe/pd bimetallic nanoparticles with sodium carboxymethyl cellulose to facilitate dechlorination of trichloroethene and soil transportability, Ind. Eng. Chem. Res. 46 (2007) 29–34.
[25] S. Si, A. Kotal, T.K. Mandal, S. Giri, H. Nakamura, T. Kohara, Size-controlled synthesis of magnetite nanoparticles in the presence of polyelectrolytes, Chem. Mater. 16 (2004) 3489–3496.
[26] H.A. Pushpadass, D.B. Ma, M.A. Hanna, Effects of extrusion temperature and plasticizers on the physical and functional properties of starch films, Starch 60 (2008) 527–538.
[27] Y. Zhang, J.H. Han, Plasticization of pea starch films with monosaccharides and polyols, J. Food Sci. 71 (2006) E253–E261.

[28] F. Jones, J.B. Farrow, W.V. Bronswijk, An infrared study of a polyacrylate flocculent adsorbed on hematite, Langmuir 14 (1998) 6512–6517.
[29] Y. Zhang, M. Yang, X-M. Dou, H. He, D-S. Wang, Arsenate adsorption on an Fe-Ce bimetal oxide adsorbent: role of surface properties, Environ. Sci. Technol. 39 (2005) 7246–7253.
[30] A. Voegelin, S. Hug, Catalyzed oxidation of arsenic(III) by hydrogen peroxide on the surface of ferrihydrite: an in situ ATR-FTIR study, Environ. Sci. Technol. 37 (2003) 972–978.
[31] M. Ristic, E. De Grave, S. Music, S. Popovic, Z. Orehovec, Transformation of low crystalline ferrihydrite to α-Fe_2O_3 in the solid state, J. Mol. Struct. 834–836 (2007) 454–460.
[32] J.T. Keiser, C.W. Brown, R.H. Heidersbach, The electrochemical reduction of rest films on weathering surface, J. Electrochem. Soc. 129 (1982) 2686–2689.
[33] S. Goldberg, C.T. Johnston, Mechanisms of arsenic adsorption on amorphous oxides evaluated using macroscopic measurements, vibrational spectroscopy, and surface complexation modeling, J. Colloid Interface Sci. 234 (2001) 204–216.
[34] G-S. Zhang, J-H. Qu, H-J. Liu, R-P. Liu, G-T. Li, Removal mechanism of As(III) by a novel Fe-Mn binary oxide adsorbent: oxidation and sorption, Environ. Sci. Technol. 41 (2007) 4613–4619.
[35] M. Pena, X. Meng, P.G. Korfiatis, C. Jing, Adsorption mechanism of arsenic on nanocrystalline titanium dioxide, Environ. Sci. Technol. 40 (2006) 1257–1262.
[36] M. Kosmulski, E. Maczka, E. Jartych, J.B. Rosenholm, Synthesis and characterization of goethite and goethite–hematite composite: experimental study and literature survey, Adv. Colloid Interface Sci. 103 (2003) 57–76.
[37] C. Su, D.L. Suarez, Selenate and selenite sorption on iron oxides: an infrared and electrophoretic study, Soil Sci. Soc. Am. J. 64 (2000) 101–111.
[38] G. Sposite, The Chemistry of Soils, Oxford Univ. Press, New York, 1989.
[39] W.F. Tan, S.J. Lu, L. Fan, X.H. Feng, J.Z. He, L.K. Coopal, Determination of the point-of-zero charge of manganese oxides with different methods including an improved salt titration method, Soil Sci. 173 (2008) 277–286.
[40] S. Biggs, Polymeric flocculants, in: P. Somasundaran (Ed.), Encyclopedia of Surface and Colloid Science, vol. 7, 2nd ed., Taylor and Francis, New York, 2006.
[41] S.A. Ravishankara, Pradip, N.K. Khosla, Selective flocculation of iron oxide from its synthetic mixtures with clays: a comparison of polyacrylic acid and starch polymers, Int. J. Miner. Process. 43 (1995) 235–247.
[42] E. Deschamps, V.S.T. Ciminelli, W.H. Holl, Removal of As(III) and As(V) from water using a natural and Mn enriched sample, Water Res. 39 (2005) 5212–5220.
[43] Z. Li, S. Deng, G. Yu, J. Huang, V.C. Lim, As(V) As(III) removal from water by a Ce-Ti oxide adsorbent: behavior and mechanism, Chem. Eng. J. 161 (2010) 106–113.
[44] F.F. Chang, J.H. Qu, H. Liu, R. Liu, X. Zhao, Fe-Mn binary oxide incorporated into diatomite as an adsorbent for arsenite removal: preparation and evaluation, J. Colloid Interface Sci. 338 (2009) 353–358.
[45] D. Zhao, A.K. SenGupta, Ligand separation with a Cu(II)-loaded polymeric ligand exchanger, Ind. Eng. Chem. Res. 39 (2000) 455–462.
[46] F. He, M. Zhang, T. Qian, D. Zhao, Transport of carboxymethyl cellulose stabilized iron nanoparticles in porous media: column experiments and modeling, J. Colloid Interface Sci. 334 (2009) 96–102.
[47] R. Kretzschmar, M. Borkovec, D. Grolimund, M. Elimelech, Mobile subsurface colloids and their role in contaminant transport, Adv. Agron. 66 (1999) 121–193.
[48] W. Hartley, R. Edwards, N.W. Lepp, Arsenic and heavy metal mobility in iron oxide-amended contaminated soils as evaluated by short- and long-term leaching test, Environ. Pollut. 131 (2004) 495–504.